



# Microstructural transitions and dielectric properties of boron-doped amorphous alumina thin film

Zhen Su<sup>1</sup>, Manwen Yao<sup>1,\*</sup>, Fei Li<sup>1</sup>, Yong Peng<sup>1</sup>, Qian Feng<sup>1</sup>, and Xi Yao<sup>1</sup>

<sup>1</sup> Functional Materials Research Laboratory, School of Materials Science and Engineering, Tongji University, No. 4800 Cao'an Road, Shanghai 201804, China

Received: 21 January 2017

Accepted: 21 April 2017

Published online:

27 April 2017

© Springer Science+Business Media New York 2017

## ABSTRACT

Dielectric  $\text{Al}_{2-x}\text{B}_x\text{O}_y$  thin films were deposited onto Pt (100)/Ti/SiO<sub>2</sub>/Si substrates via sol-gel and spin-coating technology. The microstructural transition occurred at  $\sim 500$  °C due to boron loading was confirmed by DSC and XRD. FTIR, <sup>27</sup>Al MAS NMR and XPS measurements were employed to investigate the microstructural transition caused by different boron concentrations. The results revealed that Al–O–B bonds and [AlO<sub>4</sub>] tetrahedrons were produced resulting in the reinforcement of structure with relatively low boron concentrations. With the increase of boron concentration, [BO<sub>3</sub>] chains and new surfaces crossing over the internal structure gradually produced and disrupted the structural stability. Meanwhile, hydroxyl groups were accumulated in the internal structure owing to the hydrophilic property of boron. According to the reinforced structure with low boron concentrations, the current density decreased and the breakdown strength was enhanced. Typically, the current density was decreased two orders of magnitude at 100 MV m<sup>-1</sup> and the breakdown strength of the 0.5 mol% B-doped alumina thin film was increased by 59% (from 293 to 465 MV m<sup>-1</sup>) in comparison with that of the undoped alumina thin film, whereas the dielectric properties gradually become poor due to the weak structure with the increase of boron concentration. Moreover, the dielectric constant increased owing to hydroxyl groups when the boron doping increased. This work may provide a general strategy for enhancing dielectric properties of the alumina thin film.

## Introduction

Growing demands for high-energy-density dielectric capacitors applied to power conditioning, electric launch platforms, electrical and hybrid vehicles, etc., have promoted the use of favorable dielectric materials in recent years [1, 2]. Among diverse kinds of

dielectric materials, linear dielectrics are still highly important for high density storage application [3]. Alumina (Al<sub>2</sub>O<sub>3</sub>) as the most cost-effective linear dielectric possesses a high breakdown strength (300–700 MV m<sup>-1</sup>) and stable relative permittivity (8.6–10) from DC to GHz frequencies, in conjunction with its outstanding chemical, optical and thermal

Address correspondence to E-mail: yaomw@tongji.edu.cn

stability. These merits have drawn considerable attentions to explore its potential applications in high-energy-density storage capacitors. In principle, the energy density of capacitors is proportional to dielectric constant and the square of breakdown strength ( $E$ ) for linear dielectrics [4, 5]. Meanwhile, breakdown strength is a crucial parameter to evaluate the operating limit of dielectric devices [6]. Therefore, it is important to obtain high breakdown strength and dielectric constant for achieving high energy storage density.

High breakdown strength and dielectric constant of the alumina thin film are still difficult to obtain due to structural inhomogeneities like pores, dangling bonds, and impurities caused by many reasons [7–9]. To solve this problem, foreign species, such as  $\text{Ti}^{4+}$  [10],  $\text{BaTiO}_3$  nanoparticles [11], were incorporated into the alumina thin film. However, the mechanisms of these methods are ambiguous. The network of glass is considered as a promising structure for achieving excellent high thermal stability, insulating properties and potential self-healing capacity under applied electric field [12]. Moreover, the structure can be optimized by adjusting ratios of species, such as B, Bi, Si, to obtain outstanding electrical properties [13, 14]. It is well known that boron can be easily combined with oxygen atoms to produce series of oxides with high bond strengths ( $>330 \text{ kJ mol}^{-1}$ ), including  $\text{BO}$ ,  $\text{BO}_2$ ,  $\text{B}_2\text{O}$ ,  $\text{B}_2\text{O}_2$  and  $\text{B}_2\text{O}_3$  [15]. The versatility derived from the flexibility of their atomic structure accommodates other glass formers or glass modifiers. Therefore, boron glass mixed with other glass elements possesses excellent properties and has been widely used in technology [16–18].

In this paper, the boron element (B) was introduced into the sol-gel-derived alumina thin films to tailor the microstructure by means of the flexibility and high bond strength of B–O bonds. The microstructural transition and its effect on the dielectric properties were analyzed in detail. The insight gained by this work might be helpful in designing the microstructure for enhancing dielectric properties.

## Materials and methods

### Sample preparation

The  $\text{Al}_{2-x}\text{B}_x\text{O}_Y$  ( $x = 0, 0.005, 0.02$  and  $0.1$ ) thin films (represented as B-0%, B-0.5%, B-2% and B-10%,

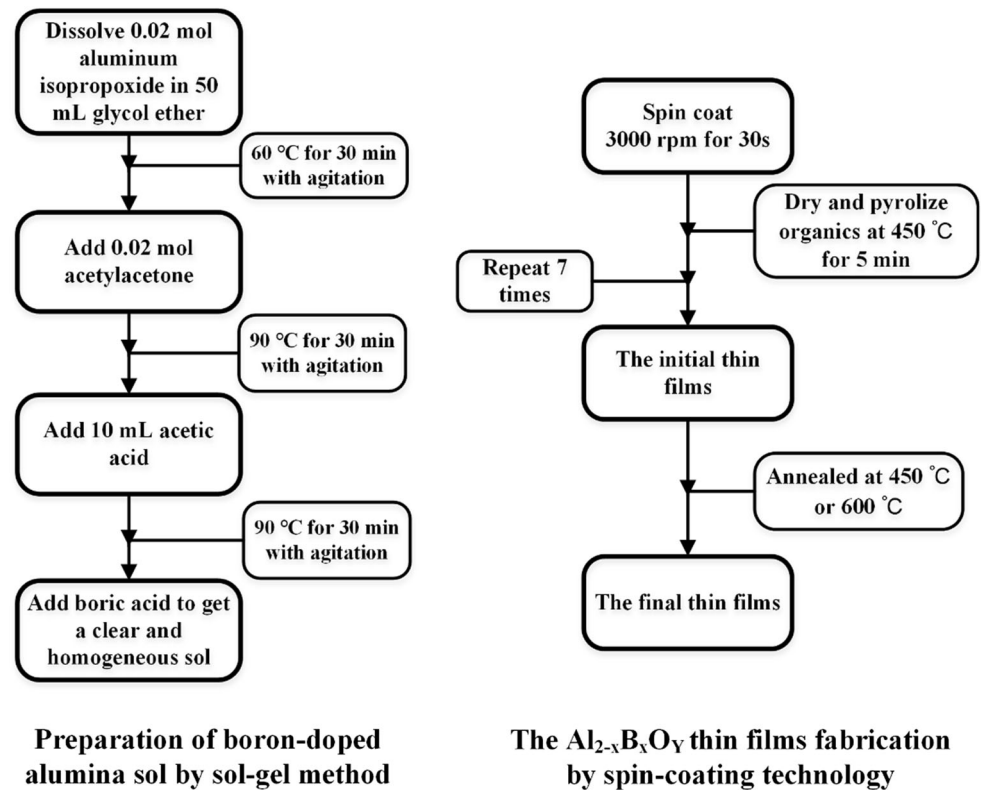
respectively) were prepared on Pt/Ti/SiO<sub>2</sub>/Si substrates by sol-gel and spin-coating technology, as seen in Fig. 1.

Boron-doped alumina sol was prepared by sol-gel method. Firstly, 0.02 mol aluminum isopropoxide was dissolved in 50 mL glycol ether, and then 0.02 mol acetylacetone, 10 mL acetic acid and appropriate ratios of boric acid were successively added to the above solutions to get a clear and homogeneous sol. The  $\text{Al}_{2-x}\text{B}_x\text{O}_Y$  ( $x = 0, 0.005, 0.02$  and  $0.1$ ) thin films were deposited on Pt/Ti/SiO<sub>2</sub>/Si substrates by spin-coating method. Each deposited film was preheated in a tubular furnace at 450 °C for 5 min for drying and pyrolysis of organics. The desired thin film thickness of approximately 210 nm was obtained after 7 times depositions in a clean-room environment. The initial thin film annealed at 450 or 600 °C (abbreviated as T-450 or T-600), for 3 h with a heating speed of 3 °C min<sup>-1</sup> to prepare the final thin films. Au top electrodes with the diameter of 1 mm were fabricated by ion sputtering onto  $\text{Al}_{2-x}\text{B}_x\text{O}_Y$  thin films for measuring dielectric properties.

### Characterizations

The combustion temperature of organics and microstructural transition temperature of the samples were recorded by differential scanning calorimeter (DSC, SAT449C, Netzsch, Germany) from 30 to 1200 °C at a heating rate of 10 °C min<sup>-1</sup> in ambient atmosphere. The structural changes of the boron-doped thin films were analyzed by X-ray photoelectron spectroscopy (XPS, ESCALAB 250Xi, Thermo Fisher, USA), Fourier transform infrared spectroscopy (FTIR, EQUINOX 55, Bruker Optics, Germany) and <sup>27</sup>Al magic-angle spinning nuclear resonance spectroscopy (<sup>27</sup>Al MAS NMR, AVANCE III HD, Bruker, Germany). Dielectric behaviors of the  $\text{Al}_{2-x}\text{B}_x\text{O}_Y$  thin film samples were measured in natural environment. The data of current density as a function of applied electric field were obtained using a source meter (Agilent 2400, USA) unit interfaced with a computer to perform the measurements. Electric field was applied in a successive voltage step of 0.2 V step<sup>-1</sup> with a delay time of 0.1 s step<sup>-1</sup>. Dielectric constant and dielectric loss measurements were taken at room temperature via a LCR meter (Agilent E4980A, USA).

**Figure 1** Flow chart of boron-doped alumina sol and  $\text{Al}_{2-x}\text{B}_x\text{O}_y$  thin films fabrication.



## Results

### Thermodynamic characteristics of boron-doped alumina sol

DSC curves of B-0%, B-0.5%, B-2% and B-10% xerogels are shown in Fig. 2. The thermal decomposition

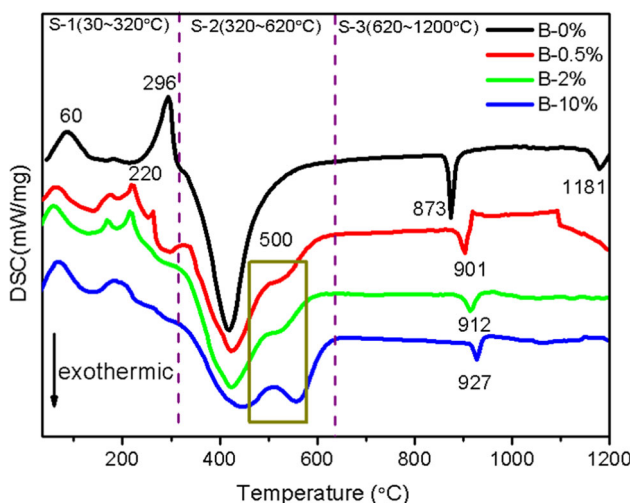


**Figure 2** DSC plots of B-0%, B-0.5%, B-2% and B-10% xerogels.

is divided into three stages. The initial stage S-1 (30–320 °C) is featured with some exothermic peaks, which are clearly associated with water desorption. The peaks at  $\sim 60$  and  $>150$  °C correspond to the loss of physical adsorption water and crystal water, respectively. In the second stage S-2 (320–620 °C), a broad exothermic peak dominates during the entire temperature ramping course and it is ascribed to the thermal decomposition of organics. It is worth noting that, unlike the DSC curve of the sample B-0%, curves of the doping films present some peaks at  $\sim 500$  °C, which become sharper with the increase of boron concentration. Combing with XRD patterns, it can be deduced that inflection points are assigned to the microstructural transition rather than crystallization because no crystallization peak except for the Pt substrate emerging after annealed at 600 °C (shown in Fig. 3). At the last stage S-3 (620–1200 °C), samples undergo primary crystallization with sharp peaks. The B-0% sample shows two exothermic peaks, due to the transitions from amorphous  $\text{Al}_2\text{O}_3$  to  $\gamma\text{-Al}_2\text{O}_3$  at 873 °C and from  $\gamma\text{-Al}_2\text{O}_3$  to  $\alpha\text{-Al}_2\text{O}_3$  at 1181 °C, respectively, whereas each B-doped sample presents only one exothermic peaks at 901, 912 and 927 °C, respectively, and they are assigned to

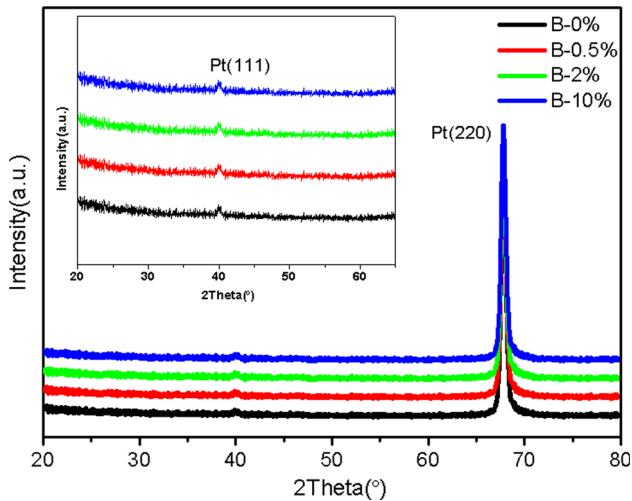


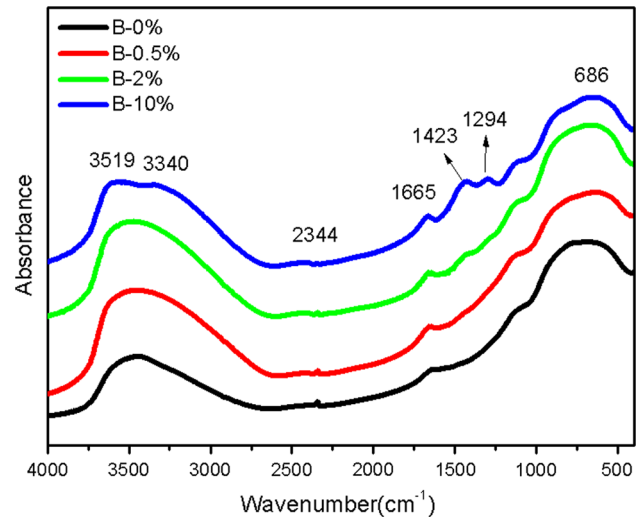
**Figure 3** XRD patterns of T-600 thin films; *inset* is the enlarged curves in the range of 20°–65°.

the transformation from amorphous alumina to  $\gamma$ - $\text{Al}_2\text{O}_3$ . Obviously, the crystallization temperature from amorphous  $\text{Al}_2\text{O}_3$  to  $\gamma$ - $\text{Al}_2\text{O}_3$  rises along with the increase of boron concentration, indicating that the addition of boron has significantly reinforced the thermal stability of the film.

### Microstructural characteristics of T-600 thin films

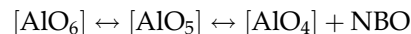
The phase and composition of T-600 thin films (including B-0%, B-0.5%, B-2% and B-10%, the same below) are examined by XRD, as shown in Fig. 3. XRD patterns exhibit two reflection peaks at  $2\theta = 39^\circ$  and  $67^\circ$ , which are assigned to (111) and (220) planes of the substrate Pt. Besides, no extra crystallization peak is observed (*inset* in Fig. 3), meaning the amorphous state of T-600 thin films.

Figure 4 shows FTIR spectra of T-600 thin films. Frequencies and their assignments for FTIR spectra of T-600 thin films are summarized in Table 1. In the study, the B–O bonds are analyzed in detail. Al–O–B bonds are formed after boron addition. With the increasing intensity of the peaks at 1294 and  $1423\text{ cm}^{-1}$ , we can know that  $[\text{BO}_3]$  units are gradually produced as boron concentration increases. The result is consistent with the Ref. [19]. Moreover, with the increase of boron concentration, a new peak of hydroxyl groups appears at  $3340\text{ cm}^{-1}$ . This may be assigned to hydroxyl groups, which exist in the new inner surfaces of thin film.



**Figure 4** FTIR spectra of T-600 thin films.

The  $^{27}\text{Al}$  MAS NMR spectra are also used to characterize the T-600 thin films in Fig. 5. Three typical peaks at  $\sim 5$ ,  $\sim 35$  and  $\sim 60$  ppm are assigned to the  $[\text{AlO}_6]$  octahedral,  $[\text{AlO}_5]$  pentacoordinate and  $[\text{AlO}_4]$  tetrahedral, respectively [26]. The  $[\text{AlO}_6]$  mainly dominates matrix structure of thin films. Meanwhile, the  $[\text{AlO}_5]$  plays a significant role in structure, suggesting that the films are amorphous [27]. The result is in accordance with XRD results. From *inset* (a) and (b), it can be observed clearly that the intensity (content) of  $[\text{AlO}_4]$  is  $I_{\text{B-0.5\%}} > I_{\text{B-2\%}} > I_{\text{B-10\%}}$  or  $0\%$  and of  $[\text{AlO}_5]$  is  $I_{\text{B-2\%}} > I_{\text{B-0.5\%}} > I_{\text{B-10\%}}$  or  $0\%$  in terms of the same  $I_{[\text{AlO}_6]}$ . Combining with the following transformation mechanisms of the aluminum polyhedron (NBO non-bridging oxygens) [28]:

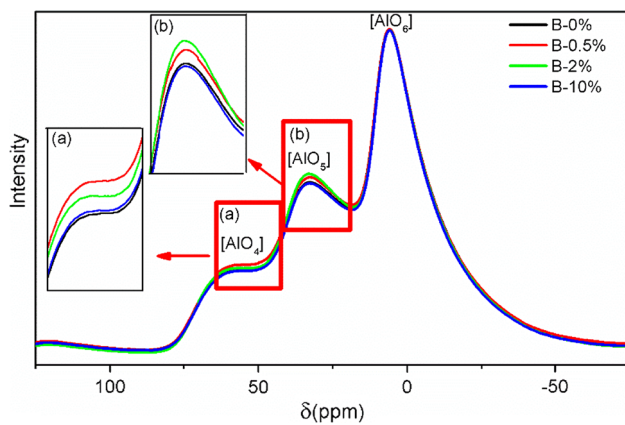
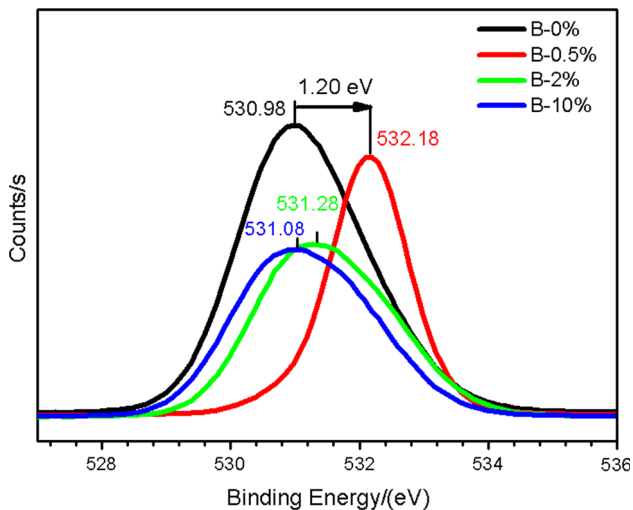


It can be seen that  $[\text{AlO}_6]$  units are more prone to transform into  $[\text{AlO}_4]$  and NBOs via pentacoordinate  $[\text{AlO}_5]$  with low boron concentrations, while increasing boron concentrations result in the suppression of the transition tendency, decrease of  $[\text{AlO}_4]$  and NBOs.

Figure 6 shows the O 1s high-resolution spectra for T-600 thin films. The main O 1s components of the T-600 films are centered at 530.98, 532.18, 531.28 and 531.08 eV, respectively. Clearly, the O 1s core level binding energy increases with boron doping. Typically, the binding energy of sample B-0.5% is dramatically 1.20 eV higher than that of the undoped alumina thin film. Moreover, the binding energy decreases with the increment of boron concentration.

**Table 1** Frequencies of their assignments for FTIR of T-600 thin films

Wavenumber (cm <sup>-1</sup> )	Assignment
450–1200 (centered at 686)	General feature of alumina and the bending information of Al–O–B bonds [20, 21]
1294	B–O asymmetric stretching vibrations in [BO <sub>3</sub> ] units from varied types of borate rings [22, 23]
1423	B–O stretching vibrations in [BO <sub>3</sub> ] units from pyro- and ortho-borate groups [22, 23]
1665	Bending vibrations of hydroxyl groups [24]
2344	Physisorbed CO <sub>2</sub> molecules [25]
2700–3700	Stretching vibrations of hydroxyl groups [24]

**Figure 5** <sup>27</sup>Al MAS NMR spectra for T-600 thin films; inset (a) is the enlarged spectra of [AlO<sub>4</sub>] region (b) is the enlarged spectra of [AlO<sub>5</sub>] region.**Figure 6** O 1s high-resolution spectra for T-600 thin films.

## Dielectric properties

Comparison of dielectric properties of T-600 thin films and dielectric properties of T-450 thin films (including B-0%, B-0.5%, B-2% and B-10%, the same

below) is investigated. Figure 7a illustrates the typical logarithmic current density ( $\log J$ ) versus the electric field ( $E$ ) of T-450 thin films. All T-450 thin films behave similarly and the current densities fluctuate in a narrow range. The current density rises sharply from  $1.0 \times 10^{-6}$  to  $2.0 \times 10^{-3}$  A cm<sup>-2</sup> with the increasing electric field ( $\leq 30$  MV m<sup>-1</sup>). At medium and high electric field region ( $>30$  MV m<sup>-1</sup>), the escalation of current density slows down, saturates and even reduces as the electric field increases. Breakdown finally occurs when the leakage current density increases sharply and abruptly. Under lower electric field, the Ohmic conduction dominates the leakage current, while the space-charge-limited current (SCLC) and Schottky emission (SE), and even other conduction mechanisms together could be the dominant conduction mechanism [29]. Since breakdown behaviors under high electric field are complicated and random, ten trails of breakdown tests have been carried out to obtain the dependable breakdown strength in this study. The measured breakdown strength follows the Weibull distribution (Fig. 7b). Breakdown strengths of B-0%, B-0.5%, B-2% and B-10% samples are 300, 308, 294 and 310 MV m<sup>-1</sup>, respectively. They do not show evident deviations. The distinctions of the T-450 thin films in breakdown strength are reasonable because many factors impact the final breakdown strength, such as defects, ambient humidity and temperature.

The  $\log J$ – $E$  characteristics and the Weibull distribution of T-600 thin films are shown in Fig. 8. When the thin films are calcined at 600 °C, the current density of B-0.5% and B-2% visibly decreases in the range of 0–200 MV/m. The current density of B-0.5% is two orders of magnitude lower than the undoped alumina thin film at 100 MV m<sup>-1</sup>. However, it is worth noting that the current density increases with the increase of boron content. The dependable breakdown strength values are obtained (Fig. 8b).

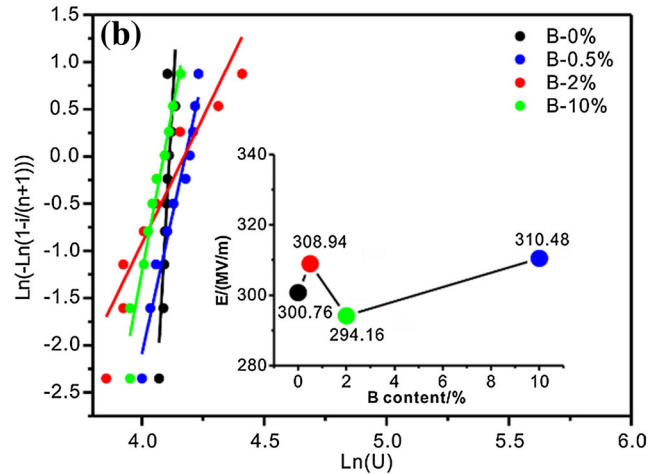
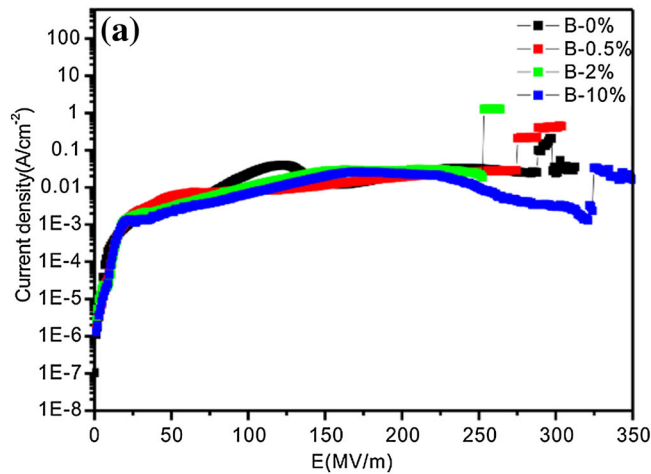


**Figure 7** **a** Log $J$ – $E$  characteristics for T-450 thin films with different boron concentrations, **b** Weibull plots of breakdown voltage of the T-450 thin films. *Inset* is dielectric breakdown strength of the samples ( $U$  is the specific breakdown voltage of

each specimen;  $n$  is the sum of specimens of each sample,  $i$  is the number of specimen, and  $E$  is the average breakdown electric field).

The breakdown strength of B-0%, B-0.5%, B-2% and B-10% in T-600 thin films is 293, 465, 414 and 312 MV m<sup>-1</sup>, respectively. Considering the impact of ambient humidity and temperature and so on, we cannot make the conclusion that the boron doping with 10 mol% makes positive influence on the breakdown strength because of the small error between B-0% and B-10%, whereas the breakdown strengths of B-0.5% and B-2% in T-600 films are enhanced compared with other samples, including all samples in T-450 films and B-0%, B-10% in T-600 thin

films. In particular, for the sample B-0.5%, the breakdown strength is increased by 59% up to 465 MV m<sup>-1</sup> compared with the undoped alumina film. Moreover, the breakdown strength decreases from 465 MV m<sup>-1</sup> to 312 MV m<sup>-1</sup> as the boron concentration increases from 0.5 mol % to 10 mol % in T-600 thin films.

The dependence of dielectric constant and dielectric loss on frequency measured at room temperature in the 100–2000 kHz range is presented in Fig. 9. The overall dielectric spectra are typical

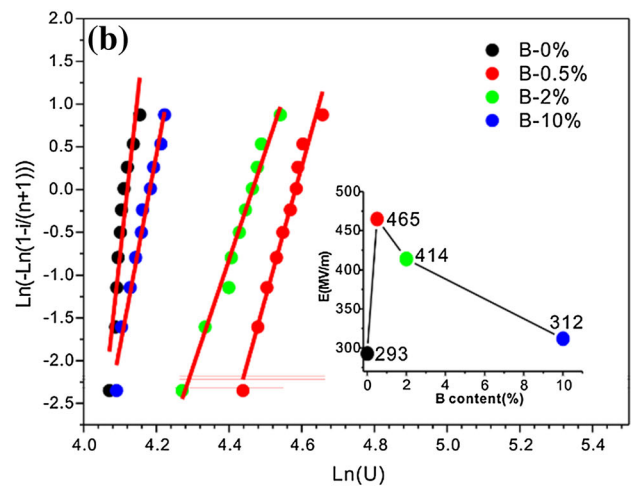
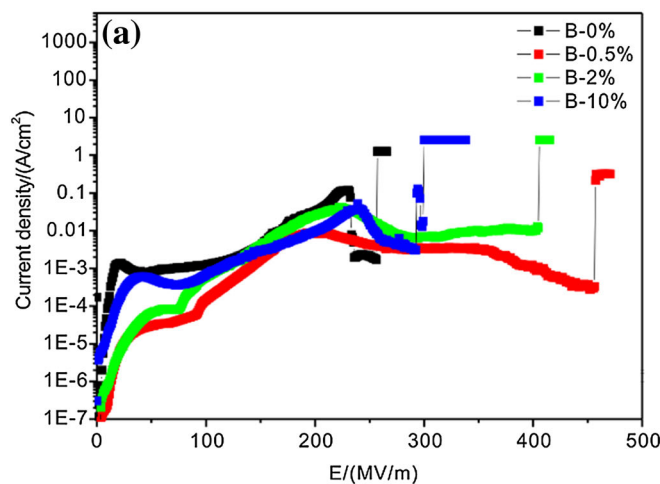


**Figure 8** **a** Log $J$ – $E$  characteristics for T-600 thin films with different boron concentrations, **b** Weibull plots of breakdown voltage of the T-600 thin films. *Inset* is dielectric breakdown strength of the samples ( $U$  is the specific breakdown voltage of

each specimen,  $n$  is the sum of specimens of each sample,  $i$  is the number of specimen, and  $E$  is the average breakdown electric field).

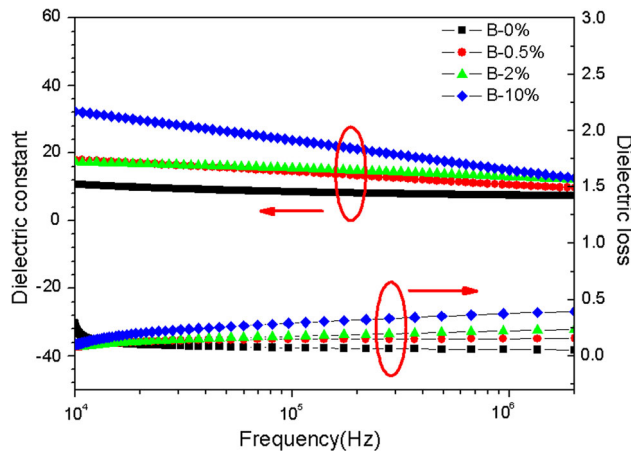


**Figure 9** Frequency dependence of dielectric constant and dielectric loss characteristics of T-600 thin films.

characteristics of conduction dominant low loss linear dielectrics. The dielectric constant decreases with the increase of frequency, whereas dielectric loss behaves in an opposite way. The incorporation of boron induces an increase in dielectric constant and dielectric loss. Meanwhile, they increase when the boron loading increases. Typically, the dielectric constant and dielectric loss increase from 17.9 to 11.2 at 50 kHz and from 0.14 to 0.39 at 2000 kHz, respectively.

## Discussion

### Microstructural transition

From the results of DSC, it is necessary to remain the annealing temperature above 500 °C for facilitating microstructural transition with boron addition. The

microstructural transition reinforces the thermal stability owing to the crystallization temperature rising from amorphous  $\text{Al}_2\text{O}_3$  to  $\gamma\text{-Al}_2\text{O}_3$  (Fig. 2). It is believed that the transition also plays a significant role in improving dielectric properties. Therefore, the correlation between the microstructural evolution and dielectric properties of the alumina thin film is investigated.

Combining with the results of FTIR, strong Al–O–B bonds are formed and participate in the framework of the amorphous alumina film. This is the reason why the thermal stability is enhanced [30]. According to Ref. [19], boron prefers to create B–O bonds, which couple each other to produce  $[\text{BO}_3]$  chains, rather replaces aluminum or occupies space to produce Al–O–B bonds in the xerogels. When xerogels are annealed above 500 °C,  $[\text{BO}_3]$  chains are partly volatilized and create new surfaces [31], as proven in Fig. 10. Figure 10 presents SEM surfaces of the (a) undoped alumina and (b) 10% boron-doped alumina thin films. Compared with the smooth and homogeneous surface of the undoped alumina thin film (Figure 10a), the surface of the 10% boron-doped alumina thin film shows some micropores and cracks, which extend to the inner of the film and create new surfaces. The unburned  $[\text{BO}_3]$  chains and newly formed surfaces are crossing over the alumina matrix that leads to a disruption of aluminum structure [32]. Meanwhile, the new surfaces are generally thought to be occupied by hydroxyl groups owing to the affinity of boron to water [18]. The boron addition affects the aluminum-oxide polyhedron as well. The  $[\text{AlO}_6]$  can be transformed into  $[\text{AlO}_4]$  and NBOs via  $[\text{AlO}_5]$  with low boron concentrations, whereas the tendency is suppressed by high boron

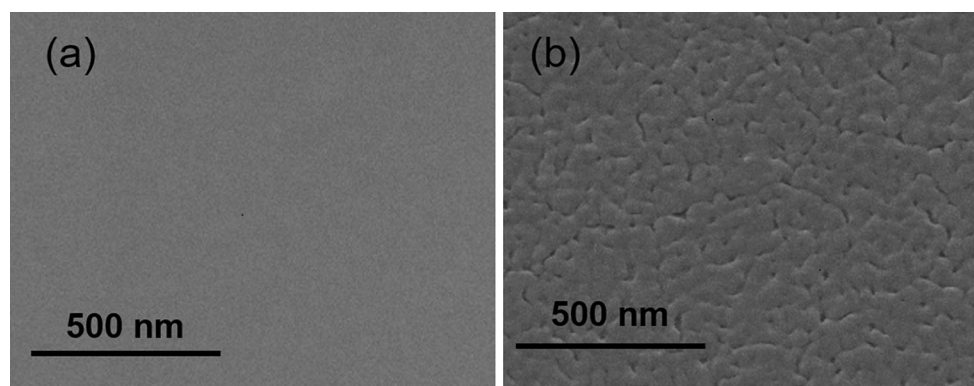


**Figure 10** SEM surface images of the **a** undoped alumina and **b** 10% boron-doped alumina thin films.

concentration (Fig. 5). The distribution of the  $[\text{AlO}_4]$  tetrahedron, which has stronger Al–O bonds than that of  $[\text{AlO}_5]$  and  $[\text{AlO}_6]$  units, can strengthen the structure.

The more structural information can be obtained from the results of XPS. It is clearly that the O 1s binding energy increases after boron addition but decreases with the increase of boron doping (Fig. 6). Owing to the high O 1s binding energy signifying the stable structure, therefore, the order of the structural stability of B-doped thin films from strong to weak is B-0.5%, B-2% and B-10%. Benefiting from the results of FTIR and  $^{27}\text{Al}$  MAS NMR, the increase of the O 1s binding energy can be assigned to newly formed strong Al–O–B bonds,  $[\text{AlO}_4]$  tetrahedrons, whereas the binding energy decrease is due to the distortion of  $[\text{BO}_3]$  chains, the suppression of  $[\text{AlO}_4]$  tetrahedrons and the tear effect of new surfaces [33, 34].

### Dielectric properties

Firstly, the current density and breakdown strength of the films before and after the microstructural transition are investigated. When the films are annealed at 450 °C, the current density and breakdown strength slightly change. While the films are annealed at 600 °C, the current densities of B-0.5% and B-2% are lower than all other thin films in the region of 0–200 MV m<sup>-1</sup>. And breakdown strengths of B-0.5% and B-2% are higher. The above phenomenon suggesting that the microstructural evolution with suitable boron contents makes the positive influence on the current density and breakdown strength. Secondly, the current density, breakdown strength and dielectric constant and loss changes of T-600 thin films caused by the incorporation of boron are analyzed. The current density, dielectric constant and dielectric loss increase as the boron concentration increasing from 0.5 to 10 mol% yet the breakdown strength decreases from 465 to 312 MV m<sup>-1</sup> (Figs. 8, 9).

The microstructural evolution allows the correlation between individual microstructural features and the dielectric properties to be determined. The dielectric properties are thought to be affected by a combination of the following factors:

- (a) Newly formed Al–O–B bonds
- (b)  $[\text{AlO}_4]$  tetrahedrons
- (c)  $[\text{BO}_3]$  chains

### (d) Hydroxyl groups

Among all thin films, the current density and breakdown strength of T-450 thin films slightly change because the microstructural evolution cannot occur. When samples are calcined at 600 °C, the lower current density and higher breakdown strength with boron doping concentrations of 0.5 and 2mol % are achieved. For the current density and breakdown strength, the changes are accompanied by the stability changes of thin films. The current density decreases with the increase of the stability. The breakdown strength increases with the increase of the stability. The B-0.5% in T-600 thin films shows the highest breakdown strength and lowest current density, which are due to the reinforced structure originating from the newly formed strong Al–O–B bonds and  $[\text{AlO}_4]$  tetrahedrons. While, as the boron doping concentration increases, the structure gradually becomes weak resulting in the increase of the current density and decrease of breakdown strength. The weak behavior is associated with  $[\text{BO}_3]$  chains dislocation and new surfaces disruption effect, produced by parts of  $[\text{BO}_3]$  chains volatilization. For the dielectric constant and loss, they all increase with the boron loading increase. The behavior may be associated with hydroxyl groups. Hydroxyl groups exist on the new surfaces and other defects of the thin films. When the higher content of boron is introduced, the larger number of hydroxyl groups is accumulated [18, 35], leading to the increase of dielectric constant and dielectric loss.

### Conclusions

In summary, amorphous B-doped alumina thin films were prepared via sol–gel and spin-coating technology. Boron doping facilitated the improvement of thermal stability and the microstructural transition occurred at ~500 °C. XRD, FTIR,  $^{27}\text{Al}$  MAS NMR and XPS measurements were employed to characterize the microstructural evolution. The results revealed that the structure was reinforced originating from the new formation of strong Al–O–B bonds and  $[\text{AlO}_4]$  tetrahedrons with relative low boron concentrations, whereas the structure turned into relatively unstable owing to the suppression of  $[\text{AlO}_4]$  tetrahedrons,  $[\text{BO}_3]$  chains dislocation and new surfaces disruption effect with the increase of boron



concentration. The microstructural transition is responsible for dielectric properties. The B-doped samples annealed at 450 °C have no obvious change in current density and breakdown strength because the microstructural transition cannot occur. However, films with boron concentrations of 0.5 and 2 mol% annealed at 600 °C exhibited significantly enhanced breakdown strength and decreased current density based on the microstructural transition. Typically, the breakdown strength of the optimum 0.5 mol% B-doped alumina thin film was increased by 59% (from 293 to 465 MV m<sup>-1</sup>) and the current density decreased two orders of magnitude at ~100 MV m<sup>-1</sup> in comparison with that of the undoped alumina thin film. With the increase of boron concentration, the structure gradually becomes weak leading to the increase of current density and the decrease of breakdown strength. Moreover, the addition of boron can increase the dielectric constant and dielectric loss due to hydroxyl groups. And they increased when the boron loading increased. The versatile dielectric properties of alumina thin film achieved by boron loading suggest a promising industrial route to prepare a flexible high-energy-density dielectric materials.

## Acknowledgements

This work is supported by the Ministry of Science and Technology of China through 973-project (Grant Number 2015CB654601) and National Science Foundation of China (Grant Number 51272177).

## Compliance with ethical standards

**Conflict of interest** The authors declare that they have no conflict of interest.

## References

- [1] Li JY, Zhang L, Ducharme S (2007) Electric energy density of dielectric nanocomposites. *Appl Phys Lett* 90:13290(1–4)
- [2] Sun P, Zhou Q, Zhu B, Wu D, Hu C, Cannata JM, Tian J, Han P, Wang G, Shung KK (2009) Design and fabrication of PIN-PMN-PT single-crystal high-frequency ultrasound transducers. *IEEE Trans Ultrason Ferroelectron Freq Control* 56:2760–2763
- [3] Peng Y, Yao M, Chen J, Xu K, Yao X (2016) Electrical characteristics of SrTiO<sub>3</sub>/Al<sub>2</sub>O<sub>3</sub> laminated film capacitors. *J Appl Phys* 120:014102(1–6)
- [4] Zhang X, Shen Y, Zhang Q, Gu L, Hu Y, Du J, Lin Y, Nan CW (2015) Ultrahigh energy density of polymer nanocomposites containing BaTiO<sub>3</sub>@TiO<sub>2</sub> nanofibers by atomic-scale interface engineering. *Adv Mater* 27:819–824
- [5] Zhu H, Liu Z, Wang F (2017) Improved dielectric properties and energy storage density of poly(vinylidene fluoride-co-trifluoroethylene-co-chlorotrifluoroethylene) composite films with aromatic polythiourea. *J Mater Sci*. doi:10.1007/s10853-016-0742-6
- [6] Neusel C, Jelitto H, Schmidt D, Janssen R, Felten F, Schneider GA (2015) Thickness-dependence of the breakdown strength: Analysis of the dielectric and mechanical failure. *J Eur Ceram Soc* 35:113–123
- [7] Neusel C, Jelitto H, Schmidt D, Janssen R, Felten F, Schneider GA (2012) Dielectric breakdown of alumina single crystals. *J Eur Ceram Soc* 3:1053–1057
- [8] Gerson R, Marshall TC (1959) Dielectric breakdown of porous ceramics. *J Appl Phys* 30:1650
- [9] Muhammad QK, Waqar M, Rafiq MA (2016) Structural, dielectric, and impedance study of ZnO-doped barium zirconium titanate (BZT) ceramics. *J Mater Sci* 51:1–11. doi:10.1007/s10853-016-0231-y
- [10] Yao M, Xiao R, Peng Y, Chen J, Hu B, Yao X (2014) The influence of titanium doping on the electric properties of amorphous alumina films prepared by sol-gel technology. *J Sol-Gel Sci Technol* 74:39–44
- [11] Yao M, You S, Peng Y (2017) Dielectric constant and energy density of poly(vinylidene fluoride) nanocomposites filled with core-shell structured BaTiO<sub>3</sub>@Al<sub>2</sub>O<sub>3</sub> nanoparticles. *Ceram Int* 43:3127–3132
- [12] Manoharan MP, Zou C, Furman E, Zhang N, Kushner DI, Zhang S, Murata T, Lanagan MT (2013) Flexible glass for high temperature energy storage capacitors. *Energy Technol* 1:313–318
- [13] Durga DK, Veeraiah N (2001) Dielectric dispersion in ZnF<sub>2</sub>–Bi<sub>2</sub>O<sub>3</sub>–TeO<sub>2</sub> glass system. *J Mater Sci* 36:5625–5632. doi:10.1023/A:1012521817440
- [14] Abdel-Wahab FA, Youssef GM, Abdallah A (2014) Electrical conduction and dielectric properties of Bi<sub>2</sub>O<sub>3</sub>–B<sub>2</sub>O<sub>3</sub>–TeO<sub>2</sub> glass. *J Mater Sci* 49:720–728. doi:10.1007/s10853-013-7753-3
- [15] Burkholder TR, Andrews L (1991) Reactions of boron atoms with molecular oxygen, infrared spectra of BO, BO<sub>2</sub>, B<sub>2</sub>O<sub>2</sub>, B<sub>2</sub>O<sub>3</sub>, and BO<sub>2</sub><sup>-</sup> in solid argon. *J Chem Phys* 95:8697–8709
- [16] Sun KH (2006) Fundamental condition of glass formation. *J Am Ceram Soc* 30:277–281
- [17] Mcpherson JW, Kim J, Shanware A, Mogul H (2003) Trends in the ultimate breakdown strength of high dielectric-constant materials. *IEEE Trans Electron Device* 50:1771–1778

- [18] Bengisu M (2016) Borate glasses for scientific and industrial applications: a review. *J Mater Sci* 51:2199–2242. doi:10.1007/s10853-015-9537-4
- [19] Dumeignil F, Guelton M, Rigole M, Amoureux JP, Fernandez C, Grimblot J (1999) Synthesis of high surface area bororia-alumina mixed oxides characterization by  $^{11}\text{B}$  and  $^{27}\text{Al}$ -NMR. *Colloid Surf Phys Eng Aspect* 158:75–81
- [20] Verlaan V, van den Elzen LRJG, Dingemans G, van de Sanden MCM, Kessels WMM (2010) Composition and bonding structure of plasma-assisted ALD  $\text{Al}_2\text{O}_3$  films. *Physica Status Solidi* 3–4:976–979
- [21] Kamitsos EI, Patsis AP, Karakassides MA, Chryssikos GD (1990) Infrared reflectance spectra of lithium borate glasses. *J Non-Cryst Solids* 126:52–67
- [22] Ardelean I, Cora S, Ciceo Lucacel R, Hulpus O (2005) EPR and FT-IR spectroscopic studies of  $\text{B}_2\text{O}_3$ - $\text{Bi}_2\text{O}_3$ - $\text{MnO}$  glass. *Solid State Sci* 71:438–1442
- [23] Ardelean I, Cora S (2007) FT-IR, Raman and UV-VIS spectroscopic studies of copper doped  $3\text{Bi}_2\text{O}_3$ - $\text{B}_2\text{O}_3$  glass matix. *J Mater Sci Mater Electron* 19:584–588
- [24] And AA, Grassian VH (2003) FT-IR study of water adsorption on aluminum oxide surfaces. *Langmuir* 19:341–347
- [25] Rege SU, Yang RT (2001) A novel FT-IR method for studying mixed gas adsorption at low concentrations:  $\text{H}_2\text{O}$  and  $\text{CO}_2$  on NaX zeolite and  $\gamma$ -alumina. *Chem Eng Sci* 56:3781–3796
- [26] Pozarnsky GA, McCormick AV (1995) Multinuclear NMR study of aluminosilicate sol-gel synthesis using the prehydrolysis method. *J Non-Cryst Solids* 190:212–225
- [27] Meinhold RH, Slade RCT, Newman RH (1993) High field MAS NMR, with simulations of the effects of disorder on lineshape, applied to thermal transformations of alumina hydrates. *Appl Magn Reson* 4:121–140
- [28] Saini A, Khanna A, Michaelis VK, Kroeker S, González F, Hernández D (2009) Structure-property correlations in lead borate and borosilicate glasses doped with aluminum oxide. *J Non-Cryst Solids* 355:2323–2332
- [29] Peng Y, Yao M, Xiao R, Yao X (2016) Electrical properties of sol-gel derived Mg-doped  $\text{Al}_2\text{O}_3$  films. *J Mater Sci Mater Electron* 27:11495–11501
- [30] Cai G, Zheng X, Zheng Y, Xiao Y, Zheng Y (2016) Synthesis of ordered mesoporous boron-doped  $\gamma$ -alumina with high surface area and large pore volume. *Mater Lett* 178:248–251
- [31] Franck Dumeignil M, Rigole A Michel, Guelton J Grimblot (2005) Characterization of bororia-alumina mixed oxides prepared by a sol-gel method. 1. NMR characterization of the xerogels. *Chem Mater* 17:2361–2368
- [32] Franck Dumeignil M, Rigole A Michel, Guelton J Grimblot (2005) Characterization of bororia-alumina mixed oxides prepared by a sol-gel method. 2. characterization of the calcined xerogels. *Chem Mater* 17:2369–2377
- [33] Fierro JLG, Peña MA, Tejuca LG (1988) An XPS and reduction study of  $\text{PrCoO}_3$ . *J Mater Sci* 23:1018–1023. doi:10.1007/BF01154005
- [34] Greaves GN, Sen S (2007) Inorganic glasses, glass-forming liquids and amorphizing solids. *Adv Phys* 56:1–166
- [35] Akerlof GC, Oshry HI (1950) The dielectric constant of water at high temperatures and in equilibrium with its vapor. *J Am Chem Soc* 72:2844–2847